Available online at www.sciencedirect.com
SCIENCE DIRECT
Annals of Nuclear Energy 33 (2006) 609–621
annals of NUCLEAR ENERGY
www.elsevier.com/locate/anucene

Power peak factor for protection systems – Experimental data for developing a correlation

Rose Mary G.P. Souza [a], João M.L. Moreira [b,*]

[a] Centro de Desenvolvimento da Tecnologia Nuclear – CDTN-CNEN/BH, Caixa Postal 941, 30123-970 Belo Horizonte, MG, Brazil
[b] Centro Tecnológico da Marinha em São Paulo – CTMSP, Av. Prof. Lineu Prestes, 2468, 05508-900 Cidade Universitária, São Paulo, SP, Brazil

Received 6 May 2005; received in revised form 6 February 2006; accepted 6 February 2006
Available online 17 April 2006

Abstract

This paper aims to construct a data set that can be used to train neural networks to furnish the power density peak factor during reactor operation. The inputs considered were those available in the reactor protection systems, namely, the axial and quadrant power differences obtained from measured ex-core detector signals, and the position of control rods. The response of ex-core detector signals was measured in experiments performed in the IPEN/MB-01 zero-power reactor. Several reactor states with different power density distribution were obtained by positioning the control rods in different configurations. The power distribution and its peak factor were calculated for each of these reactor states. The obtained results show that the power peak factor correlates well with the control rod position and the quadrant power difference, and with a lesser degree with the axial power differences. The data presented an inherent organisation and could be classified into different classes of power peak factor behaviour as a function of position of control rods, axial power difference and quadrant power difference. The analysis of the data set indicates that the power peak factor can be determined through a neural network having as input the position of control rods. Regarding only signals of ex-core detectors, the data indicate that a neural network may estimate better the power peak factor if the input vector comprises both the axial and the quadrant power differences.

1. Introduction

In this work, an investigation is carried out to improve the estimation of the power density peak factor used in the reactor control and protection systems. The objective is to obtain a set of data that would allow finding a correlation for the power peak factor using the variables available to the reactor protection system. The power density peak factor and the departure from the nucleate boiling ratio, DNBR, are monitored during operation and may cause the automatic reactor shutdown through the reactor protection system. Since they are dependent on the power density distribution, it is important to estimate it accurately because the uncertainty increases the reactor safety margins (USNRC, 1995; Lee and Chang, 2003; Na et al., 2004). Additionally, improving its accuracy brings advantages in different areas such as the implementation of simpler and more economical core loads, operating the reactor with more flexibility during load follow transients with strong axial tilts in the xenon distribution, or even increasing the plant maximum power level above the nominal value (Aragonés et al., 1996; Kuehnel et al., 2002; Meyer et al., 1978; Sipush et al., 1976).

The uncertainty margins for the protection system are usually high because the real time algorithms they use are much less sophisticated due to the need of real time processing. Normally, an algorithm for estimating the power density distribution uses measurable variables such as the ex-core detector signal, the position of control rods and, when available, the fixed in-core detector signals. The introduction of digital electronics in the design of protection systems has allowed the implementation of more intelligent and efficient algorithms to reduce the uncertainty margins placed upon the safety limits (Aragonés et al., 1996; Kuehnel et al., 2002; Lee and Chang, 2003; Kim and Chang, 1997).

The recent literature about estimating the power density distribution for protection systems is related to estimating

* Corresponding author. Tel.: +55 11 3817 7430; fax: +55 11 3817 7412.
E-mail address: jmoreira@ctmsp.mar.mil.br (J.M.L. Moreira).

0306-4549/$ - see front matter © 2006 Elsevier Ltd. All rights reserved.
doi:10.1016/j.anucene.2006.02.008

the DNBR, and uses some type of artificial neural networks technique (Kim and Chang, 1997; Guanghui et al., 2003; Lee and Chang, 2003; Na et al., 2004). It is seen applications attempting to describe the axial power density distribution with several parameters or determining the power density peak factor through axial core power differences, and position of control rods. Lee and Chang (2003) used radial basis function neural networks to estimate the DNBR in which the power distribution was estimated from the signals of ex-core detectors and position of control rods. For problems with varying power density distribution the DNBR was estimated with 10% accuracy. Seon et al. (2002) attempted, with artificial neural networks, to obtain the axial power density distribution in 20 nodes from signals of ex-core detectors. It was used simulated data to represent the ex-core detector signals and the actual power density distribution. They remarked that for an actual application to power reactors it would be necessary accurate three-dimensional power density distribution data to reduce uncertainties.

In this work, a set of data were obtained from experiments relating the power density peak factor and information from ex-core detectors and position of control rods. It was used actual signals of ex-core detectors and avoided the uncertainties that simulated data could possibly bring to the training procedures. The output data, the power peak factors, were obtained from detailed three-dimensional calculations. The experiments were performed in the IPEN/MB-01 zero-power reactor and reproduced as much as possible the actual situation found in PWRs (Moreira and Souza, 2002). Another article presents the details of the artificial neural network implementation for obtaining the power peak factor based on the training data obtained here (Souza and Moreira, 2006).

We start the article presenting in Section 2 the definitions of axial and quadrant power differences, and how these variables and the position of control rods relate with the power peak factor. Section 3 presents the experimental set-up prepared in the IPEN/MB-01 reactor, the procedures to make the measurements, the power peak factor calculations, and the obtained results. Section 4 presents the discussion of the results, and Section 5, the conclusions.

2. Power peak factor determination through neural networks

The objective of this work is to obtain a set of data that allow correlating, through the neural network technique, the power peak factor with the signals from ex-core detectors and position of control rods. In general terms, finding such a correlation, based on known results for several core states, can be viewed as finding a surface in the multidimensional space (signals of ex-core detectors, position of control rods, power peak factor) that provides the best fit to the known power peak factor results. In other words, the neural network technique provides a solution for this multidimensional curve fitting problem, where the learning process is equivalent to finding the best surface fitting in the multidimensional space, and the generalisation process is the use of this multidimensional surface to interpolate the data (Haykin, 1999; Reifman, 1997). It is clear that the quality of the training data is fundamental for a neural network correlation to produce good results. In first place the training data must be comprehensive, covering all possible scenarios that may appear later in the generalisation process. It is important to anticipate all possible power density distributions that may appear during the reactor operation and classify them into classes of similar behaviour or particular pattern (Haykin, 1999; Reifman, 1997).

The input and output variables from the training data set must resemble as close as possible the actual variables that will be involved in the generalisation process (Guanghui et al., 2003; Lee and Chang, 2003; Na et al., 2004; Kim and Chang, 1997). The variables of interest here are the ex-core detector signals, the position of control rods and the power density peak factor. We considered important that actual experimental data be used for the input variables. The position of the control rods is information that is directly measured. We avoided using simulated data for the ex-core detector signals because their response to changes in the power density distribution is difficult to model since it requires the solution of the neutron transport equation from the core region up to the detector position, across the thermal shield and pressure vessel walls (Crump and Lee, 1978). Therefore, both the position of the control rods and the signals of ex-core detectors were obtained from measurements.

It is important to train the neural networks with data which have very accurate power density distribution in order to reduce the safety margins (Seon et al., 2002). On the other hand, the power density distribution inside the core is very difficult to be measured, principally the peak factor, since it would require to have neutron detectors everywhere in the core. Since the current core design codes provide very accurate power density distributions, it was decided to use these calculated power peak factors as the output of the neural network training data.

The reported results about the utilisation of artificial neural networks to obtain the power peak factor or the DNBR indicated that the networks with the best results were those with smaller number of neurons. They also indicated that the smaller networks required smaller training data sets to yield accurate results (Guanghui et al., 2003; Lee and Chang, 2003; Na et al., 2004; Kim and Chang, 1997). Since obtaining a large and good training data set is a hard task, it seems that we should consider network topologies which are simple and with a minimum number of inputs and outputs. Networks with large number of inputs or outputs should be avoided.

2.1. Ex-core detector signals for monitoring the power density distribution

The ex-core detectors are responsible for monitoring the core power level for the control and protection systems,

and also to furnish the core axial and quadrant power differences, APD and QPD, respectively. The APD and QPD are able to observe general trends of the core power density distribution because the ex-core detectors detect only the fast neutrons coming from the core periphery that are not absorbed by the thermal shield and pressure vessel walls (Crump and Lee, 1978). Suppose that a reactor has two ex-core instrumentation channels located in its north and west sides, and that in each channel there are two detectors, one viewing the top part of the core and the other, its bottom part. Then, the axial power difference for a given channel can be defined as the difference between the signals from the detectors viewing the bottom and the top of the core, divided by the sum of both signals. For the north side, the APD^N will be

$$APD^N = \frac{C_B^N - C_T^N}{C_B^N + C_T^N} \tag{1}$$

where C_B^N and C_T^N denote the detector signals viewing the bottom and the top of the core from the north side. A similar definition can be made for the APD^W, from the core west side, by changing the superscript to "W". If the power distribution is shifted to the bottom of the core due to the presence of control rods in the top, the APD^N and APD^W will be more positive, and will be a measure of how skewed in the axial direction the power density distribution is. Due to this characteristic, APDs are commonly used to monitor strong axial tilts in the power density distribution caused by xenon poisoning transients.

The quadrant power differences for the bottom and top parts of the core indicate how asymmetric the power distribution is in the radial direction. Similarly, they can be obtained as the difference between the detector signals from the north and west sides divided by the sum of them. For the bottom part of the core,

$$QPD_B = \frac{C_B^N - C_B^W}{C_B^N + C_B^W} \tag{2}$$

The definition for the QPD_T for the top half of the core is similar.

2.2. Correlating the power peak factor to protection system variables

The power peak factor, PF, is defined as the ratio between the maximum value of the power density distribution and its average value. The core power density distribution is dependent on the position of the control rods, the xenon poisoning, burnup, and the thermal hydraulic feedback effects. The control rods, with its strong neutron absorbing nature, play the predominant role in dictating the behaviour of the power density distribution. Usually the presence of control rods in the top of the core shifts the power distribution towards the bottom, and, consequently, affects the power peak factor (Stacey, 2001). In an approximate scheme to estimate the power peak factor, it may be considered to be a function of the position of control rods,

$$PF = f_1(\text{control rods positions}) \tag{3}$$

In power reactors, the xenon poisoning causes global shifts in the power distribution in the axial direction (Stacey, 2001; Na and Upadhyaya, 1998; Sipush et al., 1976). Since it cannot be measured, the xenon poisoning effect in the power density distribution has to be monitored through the ex-core detectors. The fuel burnup cannot be measured either and must be accounted for in a similar way.

The effect of thermal hydraulic feedback on the power density distribution reduces the power peak factor due to the Doppler effect in the fuel, and shifts the power distribution to the bottom of the core due to the lower coolant temperature there. These effects may be monitored through the ex-core detector or correlating them to core state variables such as the power level or inlet and outlet temperatures. Since the thermal hydraulic feedback effects are small, it seems more appropriate to monitor them also through the ex-core detectors than to introduce more input variables in the neural network correlation.

The soluble boron is uniformly distributed in the reactor coolant and does not affect the power density distribution. It controls the core reactivity and compensates for the xenon, burnup and thermal hydraulic feedback effects. Since its concentration may vary while performing these control functions, it cannot be used to correlate the xenon or the burnup perturbations in the power density distribution.

It is seen that the burden to account for the xenon, burnup and thermal hydraulic feedback effects on the power density distribution falls over the ex-core detectors. Therefore, including examples that cover these phenomena into the data set is very important to the success of a neural network scheme to obtain the power peak factor in power reactors.

Since the APDs and QPDs bear information about the power density distribution, we can consider, as an approximation, that the power peak factor be given by

$$PF = f_2(\text{APDs}, \text{QPDs}) \tag{4}$$

The position of control rods and the APDs and QPDs have different relationships with the power peak factor. The control rods affect directly the shape of the power density distribution since it has a cause–effect relationship with the power density distribution. On the other hand, the APDs and QPDs can be considered as a rough observable of the power density distribution itself. Since they are independent variables and are monitored simultaneously by the reactor protection system, we can consider that PF be a function of all of them, that is,

$$PF = f_3(\text{control rods positions, APDs, QPDs}) \tag{5}$$

The determination of PF depends on finding the correlations f_1, f_2 or f_3, and its precision depends on how accurately these correlations can describe these relationships.

3. Measurement of the axial and quadrant power differences

The experiments were devised to provide actual data for inferring the power density peak factor out of position of

control rods and APD^W, APD^N, QPD_T and QPD_B results. In the IPEN/MB-01 reactor, a zero-power reactor, there is no xenon, burnup nor thermal hydraulic feedback effects, and only the motion of control rods can perturb the power density distribution. Different core power density distributions were obtained from different reactor critical states by changing the position of the control rods inside the core. By making specific control rod movements, some of these states emulated the xenon poisoning effect of shifting the power density distribution to both the bottom and top of the core. The minor effects of thermal hydraulic feedback and burnup were not represented.

The experimental set-up simulated the instrumentation configuration found in power reactors. Neutron detectors were positioned outside the stainless steel tank of the IPEN/MB-01 reactor to resemble ex-core power channels. For each of these critical states were measured the counts from the neutron detectors outside the moderator tank, and the position of control rods.

The power peak factors were obtained from three-dimensional core calculations which produced the k_{eff} and the power density distribution. At the end, for each core state it was registered positions of the control rods, four measured ex-core detector signals, the APDs, the QPDs, and the calculated power peak factor.

3.1. The IPEN/MB-01 reactor

The experiments were performed in the IPEN/MB-01 reactor, a zero-power light water reactor with fuel rods made of slightly enriched UO_2 pellets cladded with stainless steel (Maiorino et al., 1989). The fuel rods are individually placed in the core according to the desired geometry configuration. The assembly is located inside a stainless steel open tank full of light water which acts as the reactor moderator. The maximum core power level is 100 W corresponding to a thermal neutron flux level around 10^9 n/cm^2s.

Fig. 1 presents a top view of the core. The small squares in the figure represent the fuel rods in the assembly. Each one of the four control elements are made of 12 absorber rods connected together similarly to PWRs. They can move independently and may travel from the top to the bottom of the core. The letters "A" and "B" represent the control elements BC1 and BC2 and the letters "R" and "S" represent the control elements BS1 and BS2, respectively. The

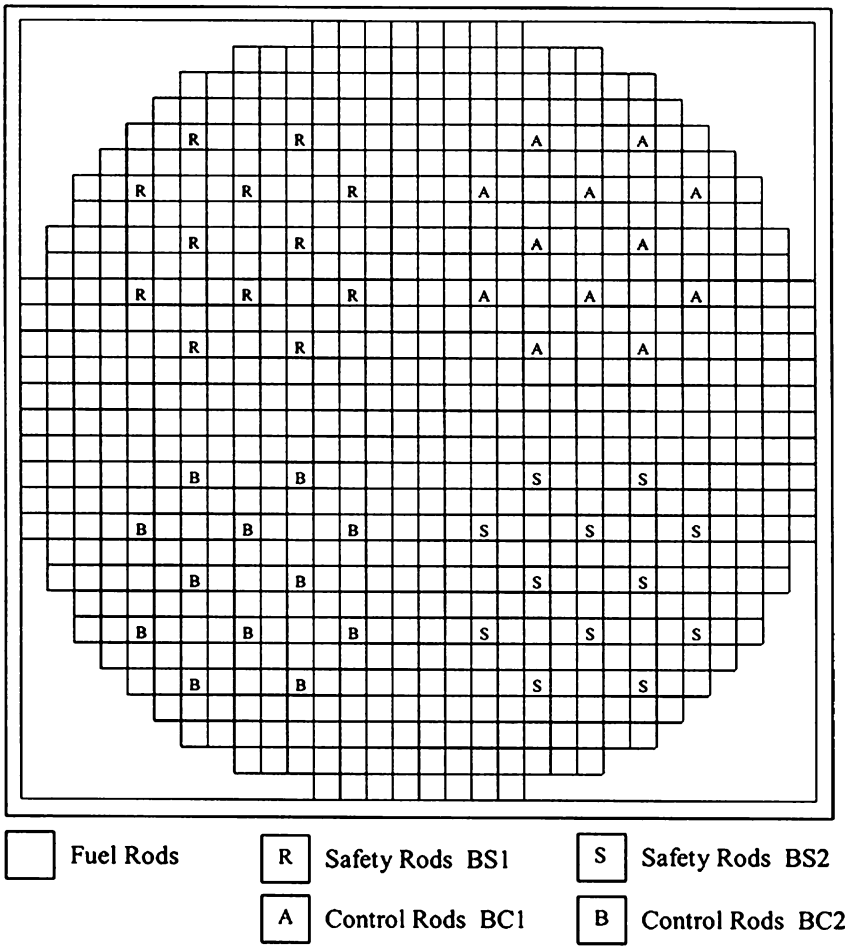

Fig. 1. Top view of the cylindrical configuration of the IPEN/MB-01 zero-power reactor core.

control elements, in spite of being formed by a set of 12 absorber rods, are also designated simply by control rods.

Fig. 2 shows a top view of the reactor with the core and the moderator tank. The large circle represents the stainless steel tank. The small circles near the core represent the several neutron detectors available for the reactor control instrumentation and for experiments. The two shaded circles outside the stainless steel tank represent the experimental ex-core detector channels located in the north and west sides of the reactor. Each channel consists of two detectors viewing the top and bottom parts of the core. Table 1 presents some technical information about the IPENB/MB-01 zero-power reactor.

Table 1
General data from the IPEN/MB-01 zero-power reactor

Parameter	Value
Fuel pellet (UO_2)diameter (cm)	0.849
^{235}U enrichment	4.3 w/o
UO_2 pellet density	94% theoretical density
Control rod absorber material	Ag (80%)–In (15%)–Cd (5%)
Control rod absorber material diameter (cm)	0.832
Safety rod absorber material	B_4C – 52% theoretical density
Safety rod absorber material diameter (cm)	0.86
Fuel and absorber rod (AISI 304) inner diameter (cm)	0.86
Fuel and absorber rod thickness (cm)	0.06
Guide tube (AISI-304) inner diameter (cm)	1.13
Guide tube thickness (cm)	0.07
Core active height (cm)	54.6
Stainless steel tank inner diameter (cm)	183
Stainless steel tank wall thickness (cm)	0.5
Instrumentation tube (aluminum) inner diameter (cm)	9.5
Instrumentation tube wall thickness (cm)	0.25
Distance between the instrumentation tube centre line and the core (cm)	18.5

3.2. Experiment to measure the ex-core detector counts

The core states with different power distributions were obtained by establishing critical configurations with different position of control rods inside the core. In order to increase the number of different states a maximum excess reactivity was obtained through the cylindrical core configuration shown in Fig. 1.

The ex-core detectors were located in symmetric positions in the west and north sides, having their centres located 18 cm above and below the core midline, as shown in Fig. 3. The neutron flux level outside of the tank is about 10^3 n/cm^2 s when the reactor is at its maximum power level, 100 W. Since this low neutron flux level required high efficiency neutron detectors, it was used ^{10}B neutron detectors as the ex-core channels. The detectors were covered with a Cd jacket with 0.114 cm thickness in order to present an active length to thermal neutrons of 18 cm. With equal active windows for all detectors, the whole experimental condition resembled more closely the ex-core instrumentation of

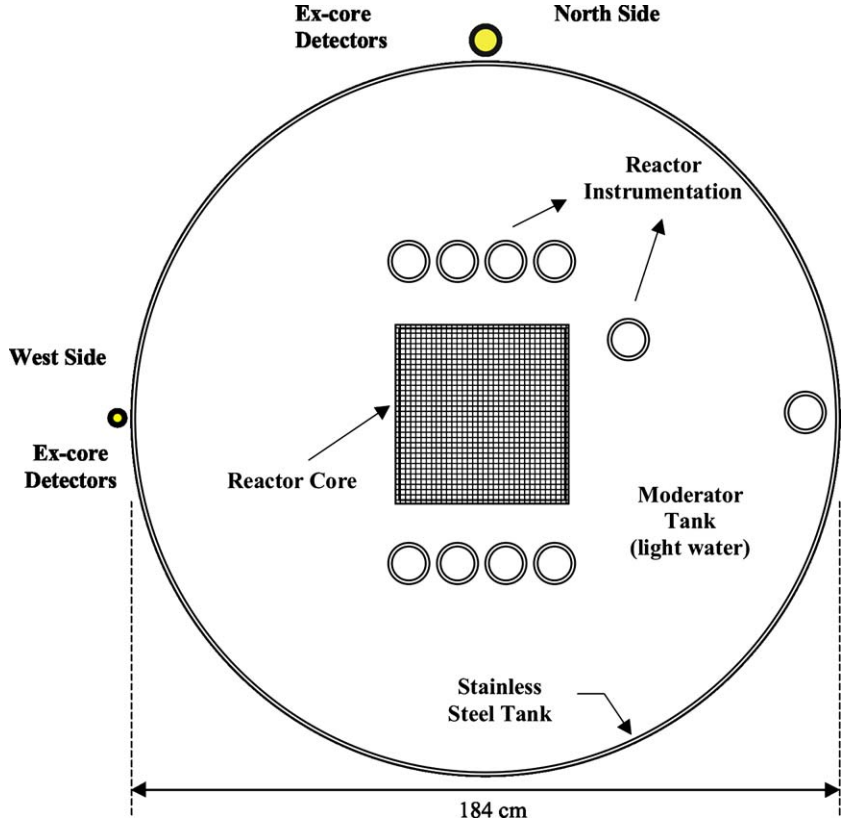

Fig. 2. Top view of the IPEN/MB-01 reactor showing the core, the moderator tank, the reactor instrumentation, and the ex-core detectors.

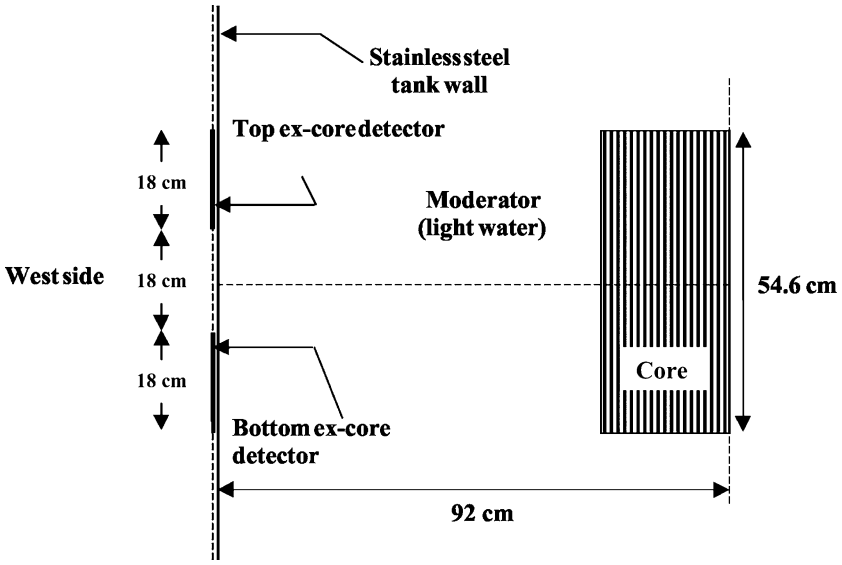

Fig. 3. Side view schematic geometry of the IPEN/MB-01 reactor showing the core, the moderator stainless steel tank and the ex-core detectors.

PWRs. Table 2 presents the technical data about the ex-core detectors set-up.

Before the measurements itself, it was obtained the sensibility of the four detectors. They were located outside the stainless steel tank at the north side bottom position, and their counts were taken at power levels ranging from 1 to 100 W. The normalisation factors obtained for the four detectors, so that they produced the same counts when located at that position, are presented in Table 2.

Fig. 2 shows that in the north side of the reactor there are four instrumentation tubes between the core and the ex-core detectors. These tubes increase the response of the detectors because of the empty volumes introduced in the region. To facilitate the analysis, the north side counts of each detector was multiplied by a constant factor in order to reproduce the counts of the west side for symmetric states. These correction factors were obtained from measurements in the state which had all the control rods positioned at the same height (state 1 in Table 4). Table 2 shows these correction factors.

Table 2
Technical data from the ^{10}B neutron detectors utilised to simulate ex-core detectors and normalisation factors

Parameter	Value
North side ^{10}B neutron detector	
Outer diameter (cm)	2.62
Total length (cm)	39.64
Active length (cm)	29.5
Cd jacketed active length (cm)	18
West side ^{10}B neutron detector	
Outer diameter (cm)	7.66
Total length (cm)	44.36
Active length (cm)	28.5
Cd jacketed active length (cm)	18
Cd jacket thickness (cm)	0.114
Normalisation factor for C_B^N	324.39
Normalisation factor for C_T^N	246.29
Normalisation factor for C_B^W	154.47
Normalisation factor for C_T^W	145.57
Correction factor for the north side count rate to compensate the empty volumes due to the reactor instrumentation	
Bottom detector	0.975
Top detector	0.733

The first core state was the one with the four control rods placed at the height corresponding to the 67.1% withdrawal position, and at 10 W power level. Then, it was taken the counts from the four detectors positioned outside the stainless steel tank. After that, similar measurements were repeated with the control rods in different configurations in order to establish different power density distributions in the core.

The control rod movements sought to emulate those that occur in PWRs during normal and abnormal operation. There are control rod motions that produce symmetric and non-symmetric perturbations in the power density distribution, regarding the ex-core detectors. The extent of control rod motion was such that covered all possible reactor states.

The control rods movements were performed in a way that the reactivity introduced in the core by the withdrawal of one or more control rods would be compensated by the insertion of other control rods in order to maintain criticality. Starting from the first state with all control rods positioned at 67.1%, one or two control rods were withdrawn to the 77.1%, 87.1% and 100% positions. In each case, the following procedure was taken to maintain criticality:

- insertion of one diagonal control rod,
- insertion of one parallel control rod,
- insertion of two control rods together.

The procedure taken to establish the several states allowed the data to be divided into 10 different classes, according to the control rod movement pattern. Table 3

Table 3
Classes of control rod motion to furnish states with different power density distributions

Class	State	Pattern of control rod movement
1	1 and 2–7	BC1 and BC2 control rods kept in a fixed position. Others compensating each other (diagonal motion)
2	1 and 8–13	BS1 and BS2 control rods kept in a fixed position. Others compensating each other (in diagonal motion)
3	1 and 14–19	BS1 and BC1 control rods kept in a fixed position. Others compensating each other (in parallel motion)
4	1 and 20–25	BS2 and BC1 control rods kept in a fixed position. Others compensating each other (in parallel motion)
5	1 and 26–31	BS2 and BC2 control rods kept in a fixed position. Others compensating each other (in parallel motion)
6	1 and 32–37	BS1 and BC2 control rods kept in a fixed position. Others compensating each other (in parallel motion)
7	1 and 38–43	BS1 and BC1 control rods move together. Others compensate together
8	1 and 44–49	BS2 and BC1 control rods move together. Others compensate together
9	1 and 50–55	BS1 and BS2 control rods move together. Others compensate together
10	56	BS2 moves compensating BS1, BC1 and BC2

shows the classes of control rod motion which were chosen in order to cover almost all possible states with different power density distribution. In order to avoid data extrapolation, for each class, the states were such that they encompassed the maximum control rod motion. Consequently, any other state with that pattern of control rod motion could have its PF result interpolated from the other states data. Altogether, 56 different critical states were established with different control rod configurations.

Table 4 presents the control rod position and the normalised ex-core detector counts for the 56 states. The experimental error regarding the control rod position is very small. The control rod position indicator has an error of $\pm 0.01\%$ or 0.0054 cm. The standard deviations presented in Table 4 for the counts are also very small, with a maximum value of $\pm 4.7 \times 10^{-3}$.

3.3. Axial and quadrant power differences results

The axial power differences, APD^N, APD^W, and the quadrant power differences, QPD_T and QPD_B, were obtained through Eqs. (1) and (2), respectively, using the detector counts presented in Table 4. Table 5 presents these results. The errors in the axial and quadrant power differences were obtained through the standard error propagation technique applied to Eqs. (1) and (2), respectively.

The values for the APDs ranged from 11.90% to 19.05% with a maximum error of $\pm 0.32\%$ (in APD^W for state 52) which is small. Comparing this maximum error with the range of variation of the APDs ($19.05\% - 11.90\% = 7.15\%$) we find that it is small, showing that the points are well defined in the domain, and that they have a good quality.

The QPDs range from -10.57% to 9.23%, with a maximum error of 0.30% which is also small (in QPD_T for state 52). Similarly, the maximum error is much smaller than the range of variation of the QPDs showing that the data have a good quality. The QPDs show many values close to zero because several states are symmetric with respect to the diagonal axis passing along the safety rods BS1 and BS2 (states from classes 1 and 9). The similar magnitude of these QPDs and their respective errors do not mean poor data since the values are close to zero.

The QPDs values indicated in Table 5 for the states belonging to classes 1 and 9 differ from zero because of the error associated to the normalisation factors which were introduced to compensate for the presence of instrumentation tubes in the north side of the core. As was mentioned before, they were obtained from state number 1.

3.4. The calculation of power peak factors

The power density distribution for each of the 56 states was obtained through a three-dimensional, four-energy groups, pin by pin, core calculation using the CITATION code (Fowler et al., 1971), a three-dimensional, multi-energy-group neutron diffusion equation code. The cross-sections were generated with a modified version of the unit cell HAMMER/TECHNION code (Barhen et al., 1978). The convergence criteria for the power density distribution in the diffusion calculation was 10^{-4}.

The PF results were obtained for the 56 states from the power density distributions produced by the CITATION code. The power peak factor results are shown in Table 5. Figs. 4 and 5 show the normalised axial power density distribution for states 40 and 43, and Figs. 6 and 7 show the normalised x–y power density distribution for the same states. It is seen that the power density distribution shifts to the west and east sides, and to the bottom, according to the control rod positions. These global shifts are similar to those produced by xenon poisoning transients in power reactors.

4. Discussion of the results

A neural network correlation requires that the training data show a meaningful relationship between the inputs and outputs. Training data are useful only if they present relationships with input and output that are clear and with identifiable patterns. The input vectors should be able to identify different states and make correct associations.

Fig. 8 presents the power peak factor as a function of the BS1 control rod position, and can be seen some type of correlation but it is not easy to be identified. The 56 states produced power peak factors ranging between 2.088 and 2.261. The power peak factor shows a relatively

Table 4
Experimental control rod positions[a] and normalised ex-core detector counts

State	BS1 (%)	BS2 (%)	BC1 (%)	BC2 (%)	$C_B^N(10^{-3})$	$C_T^N(10^{-3})$	$C_B^W(10^{-3})$	$C_T^W(10^{-3})$
1	67.10	67.10	67.10	67.10	986.8 ± 1.8	698.6 ± 1.4	987.1 ± 2.4	699.2 ± 1.9
2	59.82	77.10	67.10	67.10	943.3 ± 2.3	683.0 ± 1.9	970.6 ± 3.3	683.4 ± 2.7
3	55.86	87.10	67.10	67.10	938.9 ± 2.3	677.7 ± 1.9	964.2 ± 3.3	681.7 ± 2.7
4	53.66	100.00	67.10	67.10	937.7 ± 2.5	671.7 ± 2.0	957.7 ± 3.6	667.4 ± 2.9
5	77.10	59.81	67.10	67.10	993.2 ± 2.5	730.0 ± 2.0	1021.9 ± 3.6	724.8 ± 2.9
6	87.10	55.92	67.10	67.10	1023.2 ± 2.5	764.7 ± 2.1	1044.4 ± 3.6	752.9 ± 3.0
7	100.00	53.71	67.10	67.10	1040.5 ± 2.4	785.8 ± 2.0	1064.5 ± 3.5	779.9 ± 2.9
8	67.10	67.10	77.10	60.00	993.2 ± 2.4	725.9 ± 2.0	981.8 ± 3.4	672.7 ± 2.7
9	67.10	67.10	87.10	56.30	1007.0 ± 2.3	751.6 ± 1.9	970.4 ± 3.2	669.2 ± 2.5
10	67.10	67.10	100.00	54.33	1031.6 ± 2.5	777.6 ± 2.1	962.1 ± 3.4	670.8 ± 2.7
11	67.10	67.10	59.81	77.10	952.9 ± 2.5	670.7 ± 2.0	1021.9 ± 3.7	724.6 ± 3.1
12	67.10	67.10	55.97	87.10	971.2 ± 2.6	660.4 ± 2.0	1035.3 ± 3.9	752.3 ± 3.2
13	67.10	67.10	53.88	100.00	965.9 ± 2.7	662.2 ± 2.1	1053.0 ± 4.0	772.7 ± 3.4
14	67.10	77.10	67.10	59.13	992.1 ± 2.5	685.4 ± 1.9	970.7 ± 3.4	669.6 ± 2.8
15	67.10	87.10	67.10	55.08	995.4 ± 2.5	693.2 ± 2.0	957.4 ± 3.4	665.4 ± 2.8
16	67.10	100.00	67.10	52.85	988.5 ± 2.5	703.8 ± 2.0	953.8 ± 3.5	670.5 ± 2.8
17	67.10	61.01	67.10	77.10	986.3 ± 2.5	681.1 ± 2.0	1013.3 ± 3.6	720.6 ± 3.0
18	67.10	57.87	67.10	87.10	967.2 ± 2.6	687.9 ± 2.1	1028.7 ± 3.8	747.7 ± 3.2
19	67.10	56.18	67.10	100.00	980.5 ± 2.6	695.9 ± 2.1	1046.7 ± 3.9	766.0 ± 3.3
20	61.00	67.10	67.10	77.10	953.9 ± 2.5	660.1 ± 2.0	992.4 ± 3.6	701.2 ± 3.0
21	57.87	67.10	67.10	87.10	951.0 ± 2.6	660.4 ± 2.0	998.8 ± 3.8	715.6 ± 3.1
22	56.17	67.10	67.10	100.00	951.2 ± 2.6	659.3 ± 2.1	1007.7 ± 3.9	730.6 ± 3.2
23	77.10	67.10	67.10	59.18	1005.4 ± 2.5	712.4 ± 2.0	990.4 ± 3.4	697.9 ± 2.8
24	87.10	67.10	67.10	55.01	1048.2 ± 2.5	770.5 ± 2.1	998.0 ± 3.4	721.8 ± 2.8
25	100.00	67.10	67.10	52.79	1079.7 ± 2.6	795.2 ± 2.1	1003.8 ± 3.5	740.2 ± 2.9
26	77.10	67.10	58.96	67.10	1005.5 ± 2.5	715.3 ± 2.0	1014.4 ± 3.6	729.0 ± 3.0
27	87.10	67.10	54.91	67.10	1010.6 ± 2.5	730.7 ± 2.1	1036.8 ± 3.7	760.7 ± 3.1
28	100.00	67.10	52.61	67.10	1015.8 ± 2.6	751.3 ± 2.1	1051.8 ± 3.7	787.7 ± 3.2
29	61.02	67.10	77.10	67.10	999.5 ± 2.5	710.9 ± 2.0	969.4 ± 3.5	680.4 ± 2.8
30	57.94	67.10	87.10	67.10	1000.8 ± 2.7	730.3 ± 2.0	960.4 ± 3.4	678.3 ± 2.8
31	56.33	67.10	100.00	67.10	1015.3 ± 2.5	743.7 ± 2.1	955.1 ± 3.4	673.3 ± 2.8
32	67.10	61.05	77.10	67.10	1019.9 ± 2.5	727.7 ± 2.0	992.9 ± 3.5	701.7 ± 2.8
33	67.10	57.99	87.10	67.10	1043.9 ± 2.5	758.9 ± 2.1	992.4 ± 3.5	711.2 ± 2.9
34	67.10	56.30	100.00	67.10	1055.6 ± 2.6	783.1 ± 2.1	995.8 ± 3.5	715.4 ± 2.9
35	67.10	77.10	58.97	67.10	976.5 ± 2.5	679.0 ± 2.0	994.5 ± 3.6	700.5 ± 2.9
36	67.10	87.10	54.92	67.10	964.9 ± 2.5	673.0 ± 2.0	1001.4 ± 3.7	714.9 ± 3.0
37	67.10	100.00	52.68	67.10	962.2 ± 2.5	675.3 ± 2.0	1001.6 ± 3.7	716.0 ± 3.1
38	77.10	59.86	77.10	59.86	982.6 ± 2.4	711.2 ± 2.0	981.8 ± 3.4	703.5 ± 2.8
39	87.10	55.80	87.10	55.80	1019.7 ± 2.5	774.3 ± 2.1	996.8 ± 3.4	727.5 ± 2.8
40	100.00	53.30	100.00	53.30	1058.0 ± 2.5	832.9 ± 2.2	1008.7 ± 3.5	755.1 ± 2.9
41	59.75	77.10	59.75	77.10	882.3 ± 2.4	613.6 ± 1.9	975.9 ± 3.6	700.7 ± 3.0
42	55.62	87.10	55.62	87.10	863.9 ± 2.5	603.6 ± 2.0	992.5 ± 3.9	721.8 ± 3.3
43	53.05	100.00	53.05	100.00	862.3 ± 2.6	605.7 ± 2.1	1008.7 ± 4.1	748.9 ± 3.5
44	59.85	77.10	77.10	59.85	925.1 ± 2.3	658.4 ± 1.9	934.3 ± 3.4	649.9 ± 2.7
45	55.75	87.10	87.10	55.75	934.4 ± 2.4	682.6 ± 2.0	915.3 ± 3.4	637.0 ± 2.7
46	53.23	100.00	100.00	53.23	1026.4 ± 2.6	772.7 ± 2.2	919.9 ± 3.4	642.2 ± 2.8
47	77.10	59.77	59.77	77.10	1005.2 ± 2.8	710.2 ± 2.3	1042.8 ± 4.1	757.0 ± 3.5
48	87.10	55.63	55.63	87.10	1020.3 ± 3.0	742.4 ± 2.4	1092.3 ± 4.4	819.8 ± 3.8
49	100.00	53.05	53.05	100.00	1041.0 ± 3.1	777.0 ± 2.6	1138.9 ± 4.7	880.7 ± 4.1
50	61.22	61.22	77.10	77.10	997.2 ± 2.8	706.8 ± 2.3	989.1 ± 4.0	699.3 ± 3.3
51	58.27	58.27	87.10	87.10	1016.1 ± 2.9	731.1 ± 2.4	1000.8 ± 4.1	721.8 ± 3.5
52	56.66	56.66	100.00	100.00	1023.2 ± 3.0	756.9 ± 2.5	1014.1 ± 4.3	742.0 ± 3.6
53	77.10	77.10	59.35	59.35	1000.4 ± 2.7	707.4 ± 2.2	991.5 ± 3.9	698.1 ± 3.2
54	87.10	87.10	55.50	55.50	1017.9 ± 2.8	741.7 ± 2.3	1003.2 ± 4.0	729.8 ± 3.3
55	100.00	100.00	53.28	53.28	1025.4 ± 2.9	765.1 ± 2.4	1020.9 ± 4.1	755.6 ± 3.5
56	64.30	77.10	64.30	64.30	980.6 ± 2.7	682.4 ± 2.2	963.4 ± 3.8	672.8 ± 3.1

[a] Error in the control rod position is ±0.01% (±0.0054 cm).

flat maximum from about the 60% to the 80% control rod positions. As the control rod is moved into the core up to the 50% position, or as it is withdrawn to 100%, the PF values decrease. The power density peak factor as a function of the position of other control rods presented similar behaviour.

The behaviour shown is due to the fact that as a control rod, initially completely withdrawn, moves inside the core

Table 5
Axial power differences, quadrant power differences, and power peak factors for the 56 critical states

State	APD^N (%)	APD^W (%)	QPD_B (%)	QPD_T (%)	PF[a]
1	17.10 ± 0.13	17.07 ± 0.18	−0.01 ± 0.15	−0.05 ± 0.16	2.247
2	16.01 ± 0.18	17.37 ± 0.25	−1.43 ± 0.21	−0.03 ± 0.24	2.261
3	16.16 ± 0.18	17.17 ± 0.25	−1.33 ± 0.21	−0.29 ± 0.24	2.258
4	16.53 ± 0.20	17.86 ± 0.28	−1.06 ± 0.23	0.31 ± 0.27	2.228
5	15.28 ± 0.18	17.01 ± 0.26	−1.42 ± 0.21	0.35 ± 0.25	2.261
6	14.46 ± 0.18	16.22 ± 0.26	−1.03 ± 0.21	0.77 ± 0.24	2.258
7	13.94 ± 0.17	15.43 ± 0.24	−1.14 ± 0.20	0.38 ± 0.22	2.228
8	15.55 ± 0.18	18.68 ± 0.26	0.58 ± 0.21	3.80 ± 0.25	2.259
9	14.53 ± 0.17	18.37 ± 0.24	1.85 ± 0.20	5.79 ± 0.23	2.249
10	14.04 ± 0.18	17.84 ± 0.26	3.49 ± 0.21	7.37 ± 0.24	2.237
11	17.38 ± 0.19	17.02 ± 0.27	−3.49 ± 0.22	−3.86 ± 0.26	2.259
12	19.05 ± 0.20	15.83 ± 0.28	−3.20 ± 0.23	−6.51 ± 0.26	2.249
13	18.65 ± 0.20	15.35 ± 0.28	−4.31 ± 0.23	−7.70 ± 0.27	2.237
14	18.28 ± 0.18	18.36 ± 0.26	1.09 ± 0.22	1.17 ± 0.25	2.243
15	17.90 ± 0.18	18.00 ± 0.27	1.95 ± 0.22	2.05 ± 0.25	2.228
16	16.82 ± 0.19	17.45 ± 0.27	1.79 ± 0.22	2.43 ± 0.25	2.202
17	18.30 ± 0.19	16.88 ± 0.27	−1.35 ± 0.22	−2.82 ± 0.25	2.247
18	16.88 ± 0.19	15.82 ± 0.27	−3.08 ± 0.23	−4.17 ± 0.26	2.243
19	16.98 ± 0.20	15.49 ± 0.28	−3.26 ± 0.23	−4.80 ± 0.26	2.221
20	18.21 ± 0.19	17.19 ± 0.27	−1.98 ± 0.22	−3.02 ± 0.26	2.247
21	18.03 ± 0.20	16.52 ± 0.28	−2.45 ± 0.23	−4.01 ± 0.27	2.242
22	18.13 ± 0.20	15.94 ± 0.29	−2.89 ± 0.24	−5.14 ± 0.27	2.220
23	17.05 ± 0.18	17.33 ± 0.26	0.75 ± 0.21	1.03 ± 0.24	2.243
24	15.27 ± 0.18	16.06 ± 0.26	2.45 ± 0.21	3.27 ± 0.24	2.228
25	15.17 ± 0.18	15.12 ± 0.26	3.64 ± 0.21	3.59 ± 0.24	2.202
26	16.86 ± 0.18	16.37 ± 0.26	−0.44 ± 0.22	−0.95 ± 0.25	2.243
27	16.08 ± 0.18	15.36 ± 0.26	−1.28 ± 0.22	−2.01 ± 0.25	2.228
28	14.97 ± 0.19	14.36 ± 0.26	−1.74 ± 0.22	−2.37 ± 0.25	2.202
29	16.87 ± 0.18	17.51 ± 0.26	1.53 ± 0.22	2.19 ± 0.25	2.247
30	15.62 ± 0.19	17.22 ± 0.27	2.06 ± 0.23	3.70 ± 0.25	2.243
31	15.44 ± 0.18	17.30 ± 0.27	3.05 ± 0.22	4.97 ± 0.25	2.221
32	16.72 ± 0.18	17.19 ± 0.26	1.34 ± 0.21	1.82 ± 0.25	2.247
33	15.81 ± 0.18	16.51 ± 0.26	2.53 ± 0.21	3.25 ± 0.24	2.242
34	14.82 ± 0.18	16.38 ± 0.26	2.92 ± 0.21	4.51 ± 0.24	2.220
35	17.97 ± 0.19	17.35 ± 0.27	−0.91 ± 0.22	−1.56 ± 0.25	2.243
36	17.82 ± 0.19	16.69 ± 0.27	−1.85 ± 0.22	−3.01 ± 0.26	2.228
37	17.52 ± 0.19	16.63 ± 0.28	−2.00 ± 0.23	−2.92 ± 0.26	2.202
38	16.03 ± 0.18	16.52 ± 0.26	0.04 ± 0.21	0.54 ± 0.24	2.247
39	13.68 ± 0.18	15.62 ± 0.25	1.14 ± 0.21	3.12 ± 0.24	2.227
40	11.90 ± 0.18	14.38 ± 0.25	2.38 ± 0.21	4.90 ± 0.23	2.178
41	17.96 ± 0.20	16.41 ± 0.28	−5.04 ± 0.23	−6.63 ± 0.27	2.247
42	17.73 ± 0.21	15.79 ± 0.29	−6.93 ± 0.24	−8.91 ± 0.28	2.227
43	17.48 ± 0.22	14.78 ± 0.30	−7.82 ± 0.25	−10.57 ± 0.29	2.178
44	16.85 ± 0.19	17.95 ± 0.27	−0.50 ± 0.22	0.65 ± 0.25	2.248
45	15.57 ± 0.19	17.92 ± 0.27	1.03 ± 0.22	3.45 ± 0.26	2.228
46	14.10 ± 0.19	17.78 ± 0.28	5.47 ± 0.22	9.23 ± 0.26	2.179
47	17.20 ± 0.21	15.88 ± 0.29	−1.84 ± 0.24	−3.19 ± 0.28	2.248
48	15.76 ± 0.21	14.25 ± 0.30	−3.41 ± 0.25	−4.95 ± 0.28	2.228
49	14.52 ± 0.22	12.78 ± 0.31	−4.49 ± 0.26	−6.26 ± 0.29	2.179
50	17.04 ± 0.21	17.16 ± 0.30	0.41 ± 0.24	0.53 ± 0.28	2.215
51	16.31 ± 0.21	16.20 ± 0.31	0.76 ± 0.25	0.64 ± 0.29	2.181
52	14.96 ± 0.22	15.50 ± 0.32	0.45 ± 0.26	0.99 ± 0.30	2.142
53	17.15 ± 0.20	17.37 ± 0.29	0.45 ± 0.24	0.66 ± 0.28	2.199
54	15.70 ± 0.20	15.77 ± 0.29	0.73 ± 0.24	0.80 ± 0.28	2.151
55	14.54 ± 0.21	14.93 ± 0.30	0.22 ± 0.24	0.63 ± 0.28	2.088
56	17.93 ± 0.20	17.76 ± 0.30	0.88 ± 0.24	0.71 ± 0.28	2.248

[a] The convergence criterion for the power density distribution was 10^{-4}.

it pushes the neutron flux or the power density to the bottom of the core, causing a non-symmetric distribution with higher peak factors. After some point, the neutron flux moves to other quadrants causing a decrease in the peak factor. As the control rod is inserted even more, the neutron flux tends to return to the top of the core to attain a more symmetric distribution. For the IPEN/MB-01 reactor core configuration, we verify that as the control rod passes

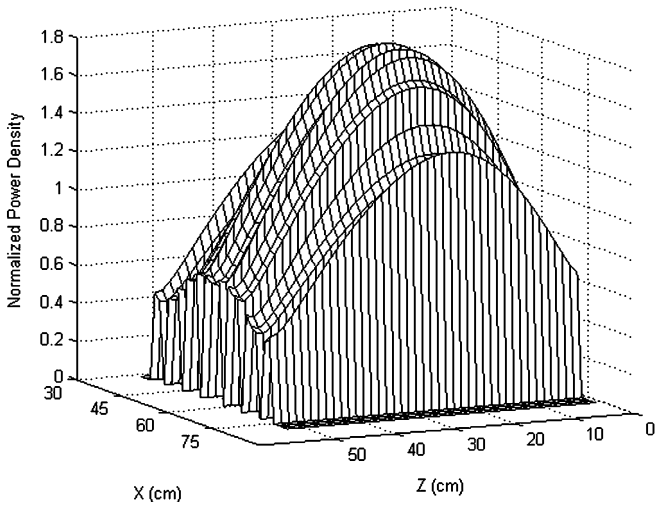

Fig. 4. Normalised axial power density distribution for state 40.

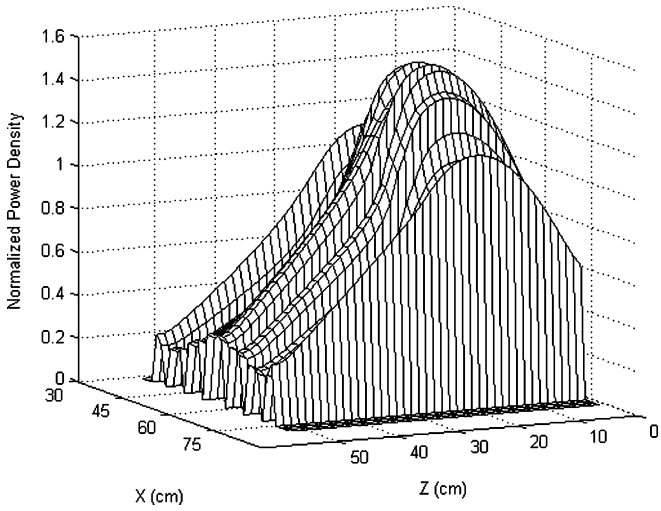

Fig. 5. Normalised axial power density distribution for state 43.

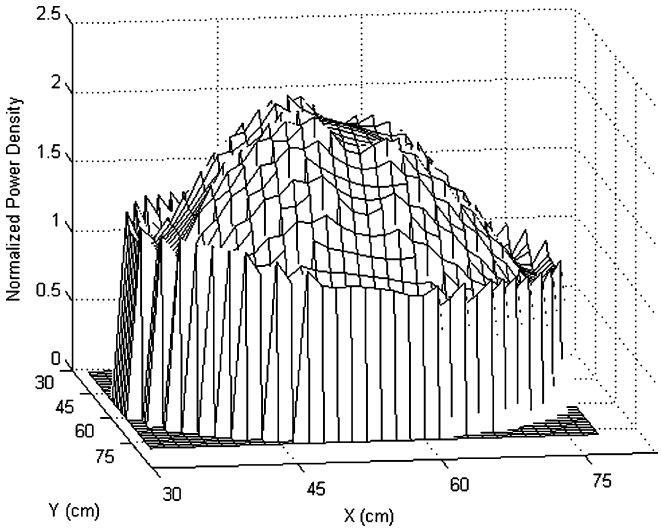

Fig. 6. Normalised x–y plane power density distribution for state 40.

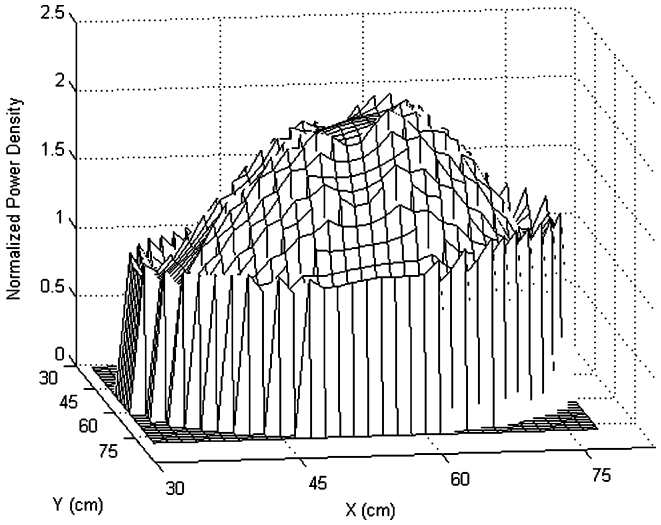

Fig. 7. Normalised x–y plane power density distribution for state 43.

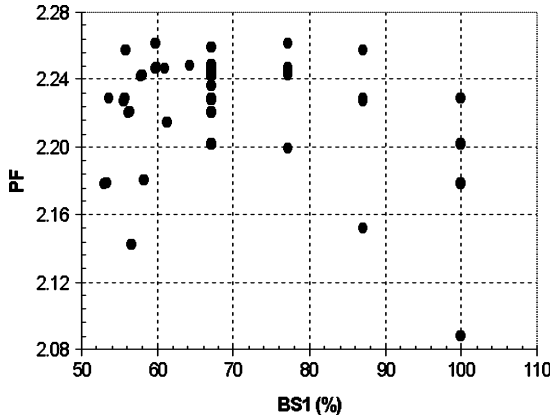

Fig. 8. The peak factor (PF) as a function of the BS1 control rod position.

about the 60% position there is the transition from pushing the neutron flux to the bottom part of the core to pushing it to the side directions.

Fig. 9 shows the same results of Fig. 8, but identifies the classes defined in Table 3 to which each state belongs. Observing Fig. 9 we can see more clearly the patterns followed by the data in each class. There are several states presenting different peak factor values but with the same control rod position. Some of them belongs to similar classes, as is the case of classes 2, 3, and 6, and others belong to different classes. This occurs because several states were obtained with one or two control rods in a fixed position and the others compensating each other in order to achieve criticality. These results indicate that, correlating the peak factor to the position of only one control rod is not sufficient to obtain a good estimate of PF. It is necessary to consider the position of the other control rods in order to identify more clearly a given core state and be able to estimate its peak factor.

Fig. 9 shows that Eq. (3) holds for each class and that is possible to find a correlation $f_1(\textit{control rods position})$ to

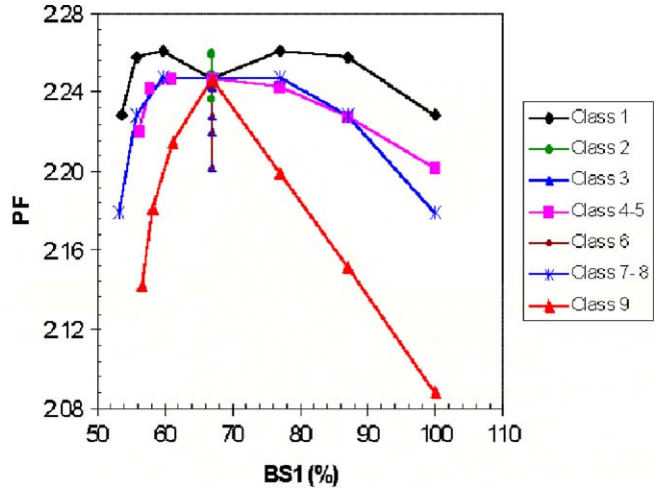

Fig. 9. The peak factor as a function of the BS1 control rod position identifying nine different classes.

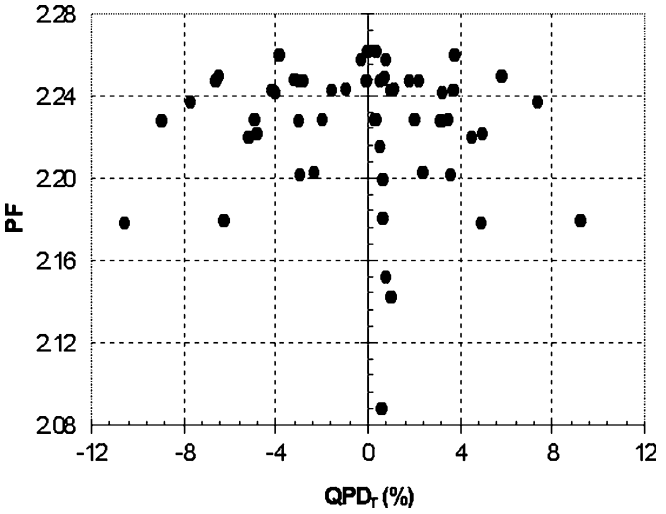

Fig. 11. The power peak factor versus the quadrant power difference for the top part of the core.

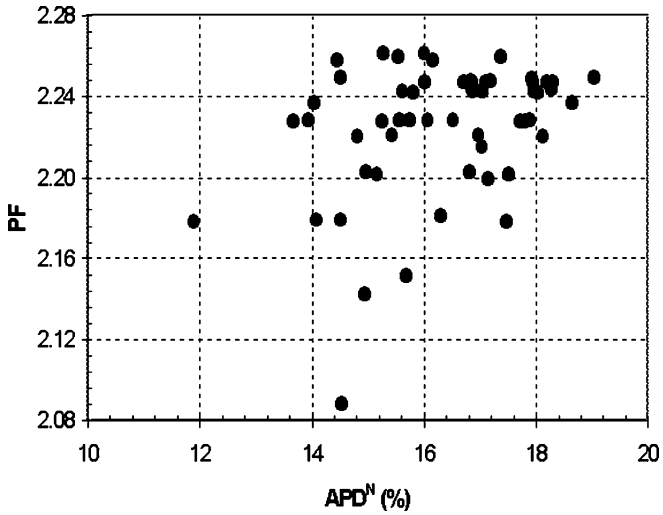

Fig. 10. Peak factor versus the axial power difference from the north side.

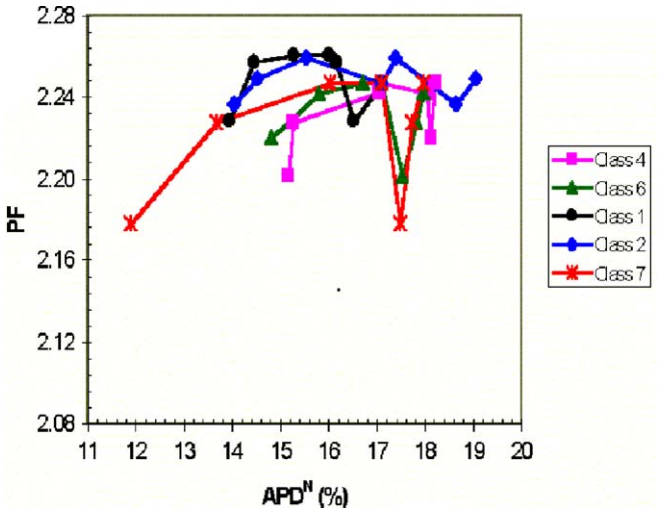

Fig. 12. The peak factor as a function of the APD^N identifying classes 1, 2, 4, 6 and 7.

obtain the power peak factor. The results presented in Fig. 9 show that the correlation between the peak factor and the control rods positions is strong, and, consequently, the data may be used to train a neural network for determining the peak factor out of control rods positions signals.

Figs. 10 and 11 present the power peak factor as a function of the APD^N and QPD$_T$ obtained from the ex-core detectors. The PF results as a function of the APD^W and QPD$_B$ present similar behaviours. The correlation between the peak factor and the APDs or QPDs is not very clear. The ex-core detectors, located far from the core, are not able to detect small differences in the power density distribution inside the core. Some states have power density distribution such that different PFs end up producing similar APDs and QPDs.

Figs. 12 and 13 reproduce Fig. 10, but identifying the classes defined in Table 3. In these figures we can follow the behaviour of PF as a function of the APD^N for each class. Except for class 9, all the others have peak factor values between 2.178 and 2.261, in the APD^N range between 11.9% and 19.05%. It appears difficult to distinguish the several classes because the PF values present irregular behaviour in that interval. This is an indication that it should be difficult to identify clearly the states using only APDs. Inside each class it is possible, with some difficulty, to follow the behaviour of PF as a function of the APD^N.

Figs. 14 and 15 show the power peak factor as a function of QPD$_T$ and identifies the class to which each data point belongs. In this case the classes have patterns more well defined indicating that the QPDs may clearly identify some states and correlate well with PF.

Observing Figs. 14 and 15, we see that classes 1 and 9 presents QPD$_T$ values close to zero. These states are symmetric with respect to the axis along control rods BS1 and BS2. The QPDs are not able to distinguish these states

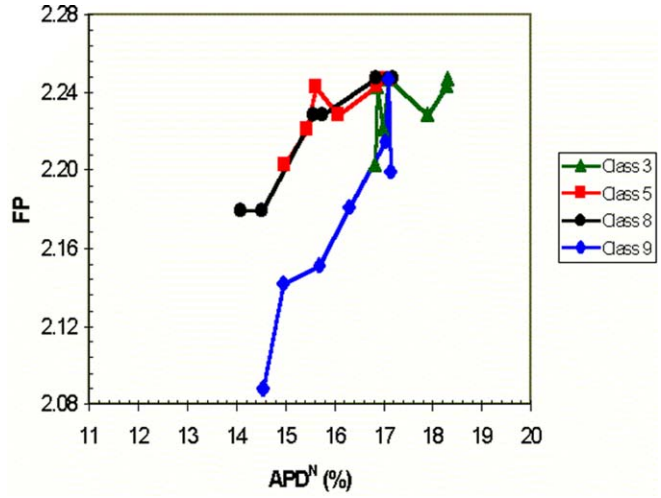

Fig. 13. The peak factor as a function of the APD^N identifying classes 3, 5, 8 and 9.

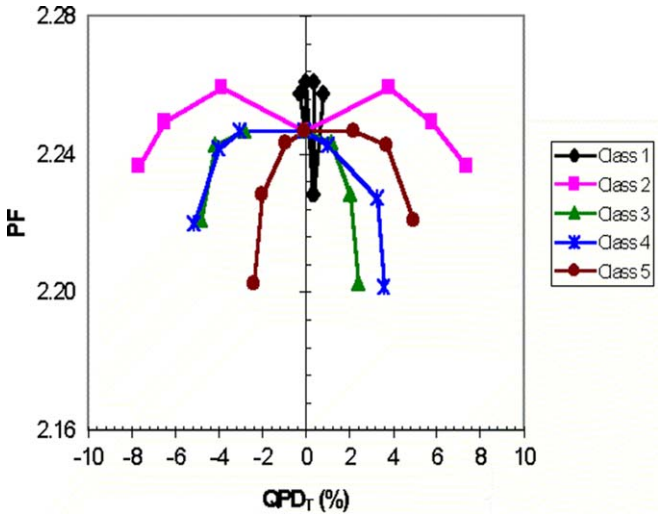

Fig. 14. The power peak factor as a function of the QPD_T identifying classes 1, 2, 3, 4 and 5.

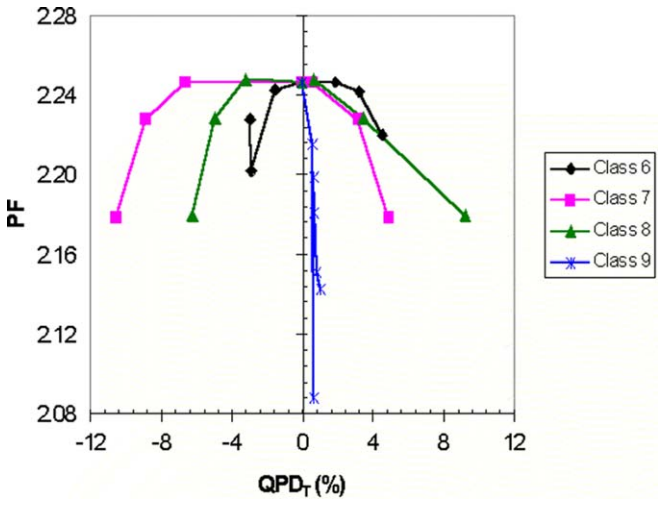

Fig. 15. The power peak factor as a function of the QPD_T identifying classes 6, 7, 8 and 9.

and, in this case, the APDs must be considered to identify them. Figs. 12 and 13 show that for classes 1 and 9, PF can be easily correlated to the APD^N.

Figs. 12–15 show that for each class Eq. (4) holds and that it is possible to find a correlation f_2(APDs, QPDs) to obtain the power peak factor. The results presented above show that there exists a correlation between the power peak factor and the axial and quadrant power differences obtained from ex-core detectors. These results show that the classes have clear patterns but it is necessary a detailed analysis of the data in order to associate the data to each class.

In power reactors, the main perturbations in the power density distribution come from the motion of control rods and from the xenon poisoning during load follow transients. It was shown that the perturbation caused by control rods could be classified into classes of similar and predictable power peak factor behaviour. For other types of perturbation, such as those due to xenon poisoning, it is also necessary that their behaviour be understood and classified into classes of similar behaviour. For power reactors, it seems that a correlation given by Eq. (5) is the best choice to obtain the power peak factor, because it contemplates in the input vector the variables bearing information about those main perturbations in the power density distribution.

5. Conclusions

This work considered the problem of developing an accurate correlation to infer the power density peak factor which can be incorporated to reactor protection systems. The artificial neural network technique was chosen to develop the correlation due to its ability to solve complex and non-linear problems in real time.

We started discussing how a neural network can account for perturbations in the power density distribution originated from control rod motion, xenon poisoning, fuel burnup and thermal hydraulic feedback. It was identified that, in power reactors, a neural network must have in its input vector information from the position of control rods, and from the signals of ex-core detectors. The control rods, with their strong neutron absorbing nature, play the predominant role in dictating the overall behaviour of the power density distribution. Axial and quadrant power differences, obtained from signals of ex-core detectors, can monitor global changes in the power density distribution such as those caused by xenon poisoning transients. The training data set must include a comprehensive set of examples contemplating the perturbations caused by the control rod motion, xenon poisoning, burnup and thermal hydraulic feedback effects on the power density distribution.

A set of training data were obtained for estimating the power peak factor using as input the position of control rods and the axial and quadrant power differences from ex-core detectors. Experiments were performed in the IPEN/MB-01 zero-power reactor to obtain a set of 56 dif-

ferent examples. Actual signals of ex-core detectors were used to obtain the axial and quadrant power differences. The experiments performed in the IPEN/MB-01 reactor reproduced as much as possible the actual situation encountered in PWRs. The power peak factors were obtained from detailed three-dimensional calculations.

The experimental results obtained in the IPEN/MB-01 reactor have shown that there is a correlation between the power peak factor and the position of control rods. The data could be divided into 10 classes of distinguished power peak factor behaviour. There was a clear pattern in their relationship which allows the position of the control rods to be used as a means to determine the power peak factor.

The experimental data have also shown that the relationship between the power peak factor and the axial power difference is more complex. The patterns for the axial power difference data are not as easy to be identified when compared to the position of control rods or quadrant power difference data. This result indicates that the axial and quadrant power difference information may be complementary in a correlation to obtain the power peak factor.

The obtained data set presented classes of behaviour in which could be identified a clear correlation between the input vector and the output. The results indicate that the data constitute a good training set for developing neural networks to estimate the power peak factor. The artificial neural network implementation based on this training data set is presented in another article.

Acknowledgments

The authors thank the Centro Tecnológico da Marinha em São Paulo, CTMSP, for funding this research work, the Centro de Desenvolvimento da Tecnologia Nuclear, CDTN, and the Instituto de Pesquisas Energéticas e Nucleares, IPEN. Thanks are also due to the technical and administrative collaboration of Hertz Pasqualetto, Rinaldo Fuga, Rogério Jerez, Alfredo Y. Abe, Hermelindo P. Manoel, Hugo M. Dalle, Leonam dos Santos Guimarães, and the reviewers.

References

Aragonés, J.M., Ahnert, C., Cabellos, O., 1996. Methods and performance of the three-dimensional pressurized water reactor core dynamics SIMTRAN On-line Code. Nuclear Science and Engineering 124, 111–124.

Barhen, J., et al., 1978. The HAMMER Code System. Technion, EPRI-NP-565.

Crump, M.W., Lee, J.C., 1978. Calculation of spatial weighting functions for ex-core neutron detectors. Nuclear Technology 41 (1), 87–96.

Fowler, T.B., Vondy, D.R., Cunninghan, G.W., 1971. Nuclear Reactor Core Analysis Code: CITATION. Rev. 2. Oak Ridge National Laboratory, Oak Ridge, TN (ORNL-2496).

Guanghui, S., Morita, K., Fukuda, K., Pidduck, M., Dounan, J., Miettinen, J., 2003. Analysis of the critical heat flux in round vertical tubes under low pressure and flow oscillation conditions. Applications of artificial neural network. Nuclear Engineering and Design 220 (1), 17–35.

Haykin, S., 1999. Neural Networks – A Comprehensive Foundation. Prentice Hall, Upper Saddle River.

Kim, H.-C., Chang, S.H., 1997. Development of a back propagation network for one-step transient DNBR calculations. Annals of Nuclear Energy 24 (17), 1437–1446.

Kuehnel, K., Richter, K.-D., Drescher, G., 2002. High local power densities permissible at SIEMENS pressurized water reactors. Nuclear Technology 137 (2), 73–83.

Lee, G.-C., Chang, S.H., 2003. Radial basis function networks applied to DNBR calculation in digital core protection systems. Annals of Nuclear Energy 30, 1561–1572.

Maiorino, J.R. et al., 1989. Projeto nuclear da unidade crítica IPEN/MB-01. In Encontro Nacional de Física de Reatores e Termo-hidráulica, VII, Recife, Brazil, April 26–28. Anais...Recife: Editora Universitária UFPE, v. 1, pp. 311–323 (in Portuguese).

Meyer, C.E., Bennett, C.L., Hill, D.J., Dzikowski, K.J., 1978. Improved load follow strategy for return-to-power capability. Nuclear Technology 41 (27), 27–35.

Moreira, J.M.L., Souza, R.M.G.P., 2002. Improving the peak power density estimation for the DNBR trip signal utilizing out-of-core detectors. In: International Symposium on Nuclear Power Plant Life Management, Budapest, Hungary, November 4–8.

Na, M.G., Upadhyaya, B.R., 1998. A neuro-fuzzy controller for axial power distribution in nuclear reactors. IEEE Transactions on Nuclear Science 45 (1), 59–67.

Na, M.G., Shin, S.H., Lee, S.M., Jung, D.W., Lee, K., Lee, Y.J., 2004. Estimation of axial DNBR distribution at the hot pin position of a reactor core using fuzzy neural networks. Journal of Nuclear Science and Technology 41 (8), 817–826.

Reifman, J., 1997. Survey of artificial intelligence methods for detection and identification of component faults in nuclear power plants. Nuclear Technology 119 (1), 76–97.

Seon, Y., Cha, C.K.H., Park, M.G., Lee, C.S., 2002. Predictive mathematical modeling for excore neutron detectors using a neural network. In: PHYSOR 2002, Seoul, Korea, October 7–10.

Sipush, P.J., Kerr, R.A., Ginsberg, A.P., Morita, T., Scherpereel, L.R., 1976. Load – follow demonstrations employing constant axial offset power – distribution control procedures. Nuclear Technology 31 (12), 12–31.

Souza, R.M.G.P., Moreira, J.M.L., 2006. Neural network correlation for power peak factor estimation. Annals of Nuclear Energy, doi:10.1016/j.anucene.2006.02.007.

Stacey, W.M., 2001. Nuclear Reactor Physics. Wiley, New York, p. 295.

USNRC, 1995. Nuclear Regulatory Commission, Standard technical specification, Westinghouse Plants, bases. Section 3.2 – power distribution limits. Rev. 1. v. 2, (NUREG-1431).